Journal of Solid State Chemistry **142,** 393–399 (1999)
Article ID jssc.1998.8054, available online at http://www.idealibrary.com on IDEAL®

Structured Diffuse Scattering as an Indicator of Inherent Cristobalite-like Displacive Flexibility in the Rare Earth Zirconate Pyrochlore $La_\delta Zr_{1-\delta}O_{2-\delta/2}$, $0.49 < \delta < 0.51$

Yasunori Tabira, Ray Withers,[1] John Thompson, and Siegbert Schmid

Research School of Chemistry, Australian National University, Canberra, A.C.T, 0200, Australia

Received July 6, 1998; in revised form September 30, 1998; accepted October 6, 1998

A detailed electron and X-ray powder diffraction study has been made of the compositional and displacive flexibility of the rare earth zirconate pyrochlore $(1-\delta)ZrO_2 \cdot \delta LaO_{1.5} = (La^{3+})_\delta(Zr^{4+})_{1-\delta}O_{2-\delta/2}$, $\delta \sim 0.5$. The extent of the pyrochlore "solid solution" in specimens rapidly quenched from 1500°C is shown to be considerably narrower than previously reported and certainly less than 2 mol.% in width. A weak but highly structured and quite reproducible diffuse intensity distribution in the form of {110}* polarized sheets of diffuse intensity perpendicular to each of the six ⟨110⟩ real space directions is observed in electron diffraction patterns and interpreted in terms of β-cristobalite-like ⟨110⟩ tetrahedral edge rotation of essentially rigid $O(2)(La)_4$ tetrahedra.

INTRODUCTION

Rare earth oxide pyrochlores, ideal stoichiometry $(Ln^{3+})_2(M^{4+})_2O(1)_6O(2)_1$ (*Ln* a lanthanide and *M* virtually any M^{4+} cation which exhibits octahedral co-ordination in a binary compound), crystallize in space group $Fd3m$ with four crystallographically independent atom sites (*Ln* in 16*d* at $\frac{1}{2}, \frac{1}{2}, \frac{1}{2}$, *M* in 16c at 000, O(1) in 48*f* at $x, \frac{1}{8}, \frac{1}{8}$, and O(2) in 8b at $\frac{3}{8}, \frac{3}{8}, \frac{3}{8}$). The structure can be described in a variety of different ways (1–3). One common description is in terms of two separate, interpenetrating network structures (see Fig. 1). The first network (see Fig. 1 (top)) is an $(M^{4+})_2O(1)_6$ array of corner-connected, cation-centred "octahedra" while the second network (see Fig. 1 (bottom)) is an $O(2)(Ln^{3+})_2$ array of corner-sharing, oxygen-centered tetrahedra (the anti-type structure to the "ideal" β-cristobalite structure type). An alternative more fluorite-based description is in terms of a metal ion ordered, ccp eutactic cation array with O(1) ions occupying off-center sites within Ln_2Zr_2 tetrahedra and O(2) ions Ln_4 tetrahedral sites therein (2, 3).

[1]To whom correspondence should be addressed.

The one free positional parameter, the *x* fractional coordinate of O(1), is important in that it determines how far O(1) ions are displaced from the centers of Ln_2Zr_2 tetrahedra and consequently the extent to which the six- and eight-fold coordination polyhedra surrounding the *M* and *Ln* cations are distorted from octahedral and cubic coordination respectively. For a regular octahedral oxygen environment around *M*, *x* should be 0.3125, whereas, for a regular cubic oxygen environment around *A*, *x* should equal 0.375. In practice, *x* tends to be smallest for the largest rare earth ion and ranges from 0.319 to 0.343 for rare earth oxide pyrochlores (2, 3).

For the lower *x* values, the considerable reduction from the ideal fluorite value of 0.375 leads toward a puckered hexagonal bipyramidal coordination for the rare earth ions (with two rather short *Ln*–O(2) bonds and six rather longer *Ln*–O(1) bonds) and to very anisotropic atomic displacement parameters for the Ln^{3+} ion (2, 3). In conjunction with often rather short *Ln–Ln* separation distances, this suggests that $O(2)(Ln^{3+})_4$ tetrahedra should, to a good approximation, vibrate as rigid units. Solid evidence for the existence of such rigid unit modes has, however, yet to be produced.

Stability field diagrams (2, 3) show that virtually any M^{4+} cation which exhibits octahedral coordination in a binary compound can be found in one or another pyrochlore compound. When the M^{4+} cations become sufficiently large relative to the rare earth ions (in practice only for M = Zr or Hf), significant ranges of stoichiometry on either side of the ideal $Ln_2M_2O_7$ composition and order–disorder transformations at high temperature from pyrochlore to disordered "defect fluorite" have been reported, although it should be noted that the various reported pyrochlore solid solution widths and composition ranges are not in good agreement with one another (2–10). Rare earth zirconates of stoichiometry $(Ln^{3+})_\delta(Zr^{4+})_{1-\delta}O_{2-\delta/2}$, $\delta \sim 0.5$, are reported to have the ideal pyrochlore structure up to relatively high temperatures for the lighter lanthanides ranging from La to Gd (8) but to transform to a disordered "defect

0022-4596/99 $30.00

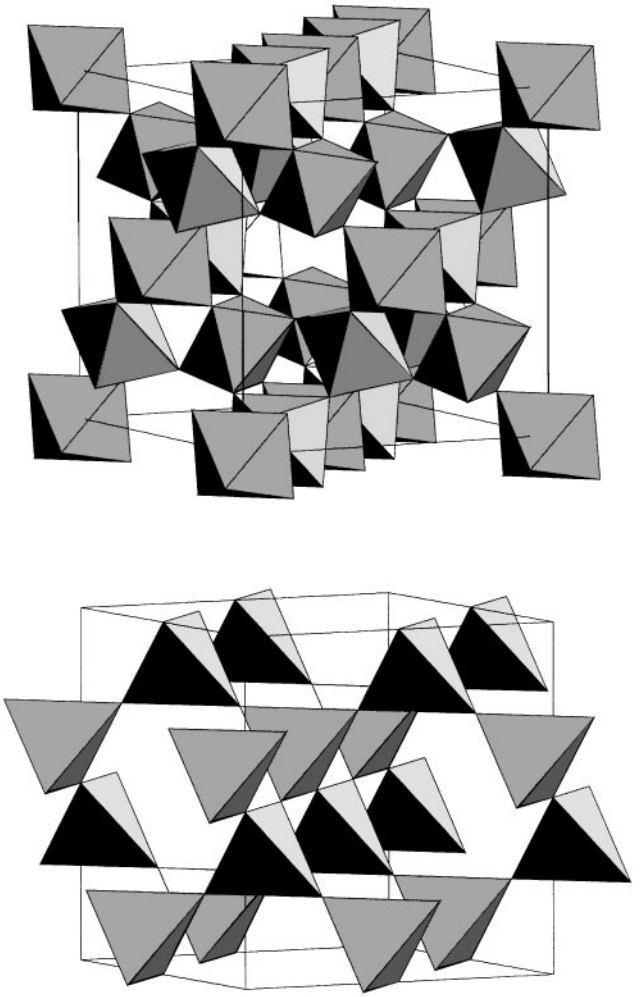

FIG. 1. The two interpenetrating network structures that together constitute the pyrochlore structure type. The first network (top) is an $(M^{4+})_2O(1)_6$ array of corner-connected, cation-centered "octahedra" while the second network (bottom) is an $O(2)(Ln^{3+})_2$ array of corner-connected, oxygen-centered tetrahedra (of "ideal" anti-β-cristobalite structure type).

fluorite" phase at still higher temperatures (except in the case of $Ln = La$, where the pyrochlore phase is stable up until the melting point). For the heavier lanthanides beyond Gd, only the disordered defect fluorite phase is found (8).

As part of an ongoing investigation into compositional and/or displacive structural flexibility in fluorite-related zirconates, this paper presents the results of a transmission electron microscope (TEM) and X-ray powder diffraction (XRPD) study of the rare earth zirconate pyrochlore $(La^{3+})_\delta(Zr^{4+})_{1-\delta}O_{2-\delta/2}$, $\delta \sim 0.5$.

EXPERIMENTAL METHODS

Samples were prepared by grinding La_2O_3 (Amer. Potash and Chem. Co., 99.99%) and ZrO_2 (Cerao, Inc., 99.7%) in the appropriate ratio close to 1 : 2, pelleting and calcining. Because freshly prepared La_2O_3 is so hygroscopic (transforming to $La(OH)_3$ within several hours upon standing at room temperature), fresh La_2O_3 was prepared from the nominal La_2O_3 by heating overnight at 1000°C prior to weighing. Initially the pellets were placed on alumina tiles for calcination. It was found, however, that the La_2O_3 invariably reacted with the alumina tiles, giving rise to a β-alumina impurity phase in addition to the desired reaction products. Stabilized zirconia crucibles were therefore substituted for alumina tiles at the calcination stage and no further problems were thereafter encountered with respect to unwanted impurity phases.

The ground samples were typically calcined at 1500°C for 72 h in the stabilized zirconia crucibles, reground, and reheated (for a further 72 h) prior to rapid quenching in water. XRPD data from the quenched samples were collected using a Guinier–Hägg camera with monochromated Cu$K\alpha_1$ radiation. ThO_2 ($a = 5.5958(3)$ Å) was added as an internal standard for the determination of unit cell dimensions. Electron diffraction patterns (EDPs) were recorded using a Philips EM430 TEM. The specimens were prepared by crushing and dispersing onto holey carbon-coated copper grids.

RESULTS

Initial Powder XRD Investigation

The pyrochlore solid solution in the $(1-\delta)ZrO_2 \cdot \delta LaO_{1.5}$ system has variously been reported as extending from 49 to 57 mol.% $LaO_{1.5}$ (4), from 48 to 56 mol.% (7) and, most recently, from 44 to 52 mol.% (8) at 1500°C. In order to more accurately determine the width and compositional range of the pyrochlore solid solution field, albeit at only one temperature, samples were prepared at compositions ranging from 40 to 60 mol.% $LaO_{1.5}$ in 2.5 mol.% steps. Quenching samples from 1500°C gave white-colored specimens at the lower $LaO_{1.5}$ contents up to 50 mol.%. Beyond 50 mol.% the specimens gradually took on a brown hue.

In general agreement with the most recently reported phase diagram (8), specimens at the lower $LaO_{1.5}$ content were found via XRPD to be in a pyrochlore plus monoclinic zirconia two phase region while specimens at the higher $LaO_{1.5}$ content were found to be in a pyrochlore plus A-type sesquioxide two phase region. The strongest peaks of the monoclinic zirconia phase were clearly present in the 40, 42.5, and 45 mol.% specimens and weakly, but still clearly, present in the 47.5 mol.% $LaO_{1.5}$ specimen. Similarly the strongest peaks of the A-type sesquioxide were found to be present in each of the 60, 57.5, 55, and 52.5 mol.% specimens. In an effort to define the pyrochlore solid solution more tightly, two further specimens were then prepared at 49 and 51 mol.% $LaO_{1.5}$. No monoclinic zirconia or A-type sesquioxide lines could be detected visually in either of these specimens.

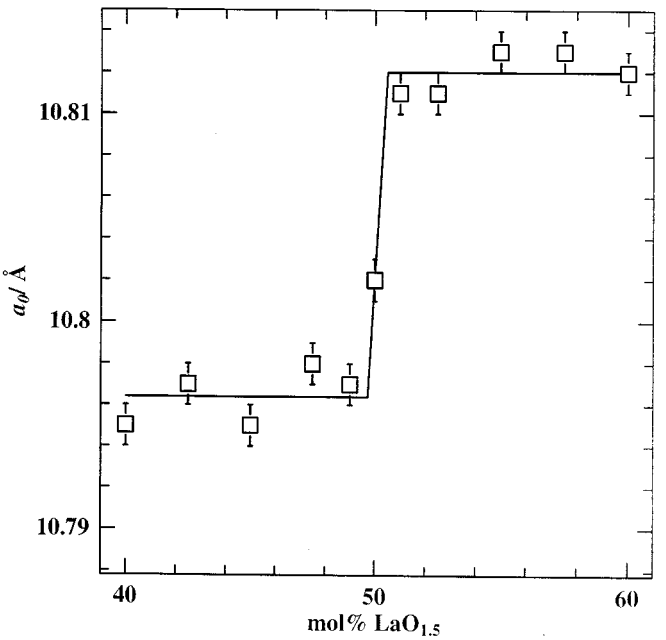

FIG. 2. Refined unit cell dimensions of pyrochlore type $(1-\delta)ZrO_2 \cdot \delta LaO_{1.5} = (La^{3+})_\delta(Zr^{4+})_{1-\delta}O_{2-\delta/2}$ as a function of composition.

The refined pyrochlore cell parameter as a function of composition (see Fig. 2) shows that the extent of the pyrochlore solid solution at 1500°C is considerably narrower than previously reported and certainly less than 2 mol.% in width. The end member pyrochlore unit cell dimension on the lower $LaO_{1.5}$ side is 10.796(2) Å while that on the higher $LaO_{1.5}$ side is 10.812(2) Å. The rather small difference ($\sim$0.016 Å) between these end member pyrochlore unit cell dimensions is consistent with an extremely narrow solid solution in the Ln = La case. In the $(1-x)ZrO_2 \cdot xPrO_{1.5}$ system (9), by contrast, the end member pyrochlore cell dimension on the lower $LnO_{1.5}$ side (at $x \sim 0.47$) is $\sim$0.11 Å less than that of the cell dimension at $x = 0.50$ while the difference in end member lattice parameters in the case of Ln = Nd is $\sim$0.2 Å (10). It would appear that the width of the pyrochlore solid solution increases, rather than decreases (11), in going from Ln = La to Gd.

Electron Diffraction Investigation of $La_2Zr_2O_7$

Given the widely accepted interpenetrating B_2O_6 and OA_2 network description of the $A_2B_2O_7$ pyrochlore structure type (see Fig. 1; (2, 3) and references contained therein) with its apparent implication of more or less rigid BO_6 octahedra and OA_4 tetrahedra, we were at first rather surprised to find that reciprocal space in the case of $La_2Zr_2O_7$ was characterized by the existence of a weak but highly structured and quite reproducible diffuse intensity distribution in addition to the sharp Bragg reflections of an underlying pyrochlore type average structure (see Fig. 3). (The weakness of this diffuse distribution relative to the strong Bragg reflections of the average pyrochlore structure meant that it was often difficult to record at major zone axis orientations unless one either tilted slightly away from the exact zone axis orientation in order to reduce the intensity of the Bragg reflections excited in the zero order Laue zone (ZOLZ) or, alternatively, burnt out the ZOLZ portion of the pattern). The existence of such a diffuse distribution implies highly correlated, displacive structural flexibility despite the supposed rigidity (2) and overdetermined nature of the pyrochlore structure type (12).

The diffuse distribution takes the form of polarized $\{110\}$* sheets of diffuse intensity. Fig. 3, for example, shows (a) $\langle 111\rangle$, (b) $\sim\langle 112\rangle$, (c) $\langle 543\rangle$, and (d) $\langle 314\rangle$ zone axis EDPs characteristic of stoichiometric $La_2Zr_2O_7$ specimens. In each case note the presence of diffuse streaking along $\langle hhl\rangle$* directions of reciprocal space. Polarized $\{110\}$* sheets of diffuse intensity (perpendicular to the $\langle 110\rangle$ directions of real space) imply the existence of $\langle 110\rangle$ columns of atoms whose motion is totally correlated along $\langle 110\rangle$ but completely uncorrelated perpendicular to $\langle 110\rangle$ (14–17).

Note further the fact that the intensity of this diffuse streaking is always strongest along directions of reciprocal space perpendicular to the direction of the diffuse streaking itself. Such azimuthal intensity variation requires, first, that atomic displacements must be largely responsible for the observed diffuse distribution and, second, that these atomic displacements must be largely polarized perpendicular to the observed $\{110\}$* sheets of diffuse intensity, i.e., along the $\langle 110\rangle$ directions of real space. Such a situation is strongly reminiscent of the β-, or high temperature, form of the SiO_4 tetrahedrally corner-connected cristobalite polymorph of silica (14, 15), which also has the same average structure space group symmetry and a diffuse intensity distribution which is also characterized by similarly polarized sheets of diffuse intensity perpendicular to the $\langle 110\rangle$ directions of real space (cf., for example, the $\langle 112\rangle$ zone axis EDP of β-cristobalite in Fig. 4 with the $\sim\langle 112\rangle$ zone axis EDP of $La_2Zr_2O_7$ shown in Fig. 3b). Such analogous behavior is by no means a coincidence.

In the case of β-cristobalite, the polarized sheets of diffuse intensity perpendicular to $\langle 110\rangle$ have been shown to arise from coupled rotation of the SiO_4 framework tetrahedra about their $\langle 110\rangle$ tetrahedral edges (see Fig. 5). Such tetrahedral edge rotation is the natural "normal mode" for β-cristobalite-type framework structures (14–17). Only one $\langle 110\rangle$ column of tetrahedra is shown in Fig. 5 because the connectivity of these columns in the β-cristobalite structure type is such that the sense of rotation from one column to the next is not determined by the sense of rotation of the initial column. This lack of correlation in the sign of the tetrahedral edge rotation from one $\langle 110\rangle$ column to the next is responsible both for the observed diffuse intensity

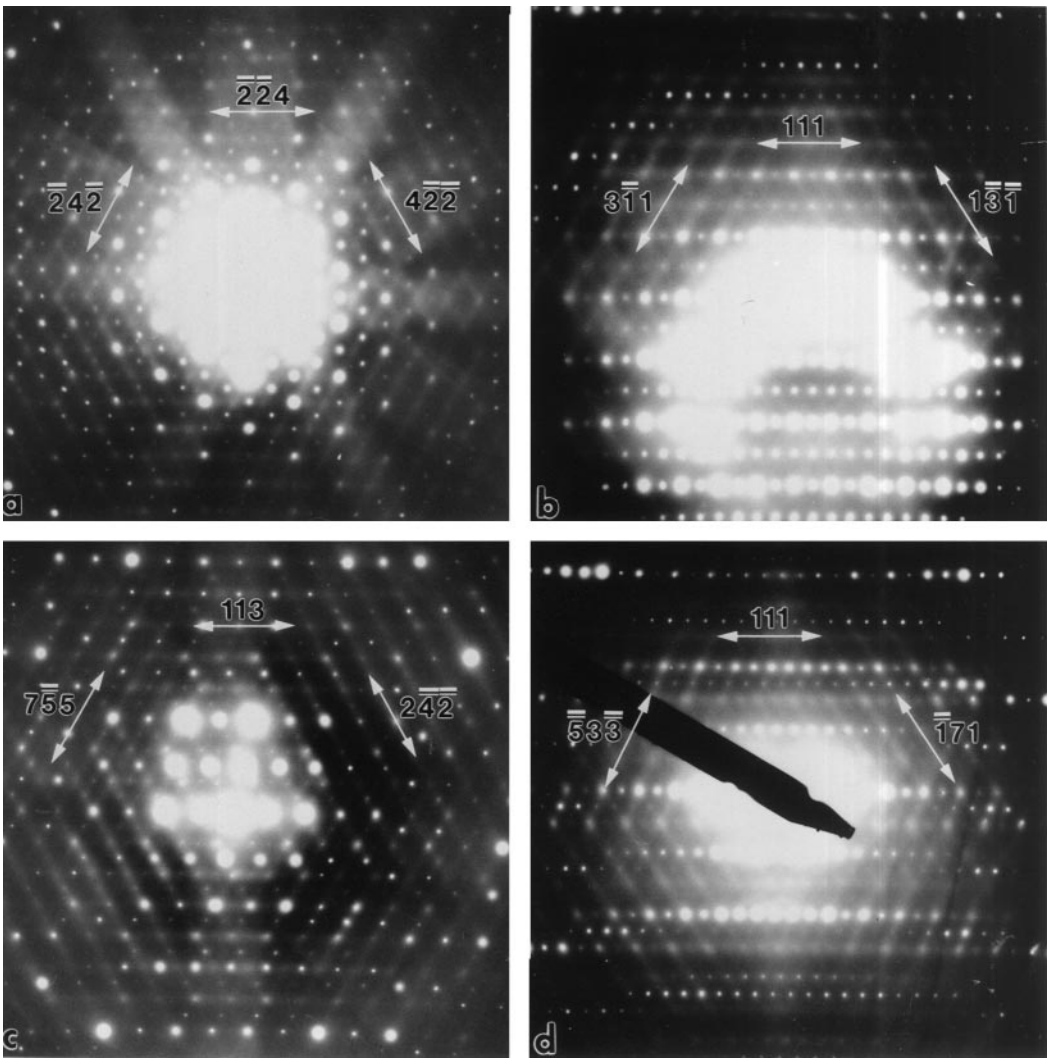

FIG. 3. (a) ⟨111⟩, (b) ~⟨112⟩, (c) ⟨543⟩, and (d) ⟨314⟩ zone axis EDPs characteristic of stoichiometric $La_2Zr_2O_7$. In each case note the presence of polarized diffuse streaking along ⟨*hhl*⟩* directions of reciprocal space.

distribution characteristic of β-cristobalite (14–17) and for the virtual infinity of different possible derivative structures.

The existence of a similar OLa_2 anti-β-cristobalite-type framework as one of the two interpenetrating networks comprising the pyrochlore structure (see Fig. 1b and Refs. (1–3)) strongly suggests that the observed diffuse scattering in $La_2Zr_2O_7$ must likewise arise as a result of similar coupled rotation of essentially rigid OLa_4 tetrahedra about their ⟨110⟩ tetrahedral edges (see Fig. 5). As for β-cristobalite, it is proposed that the lack of correlation in the sign of the tetrahedral edge rotation from one ⟨110⟩ column to the next is responsible both for the observed diffuse intensity distribution and for the average cubic space group symmetry.

A complication in the case of the pyrochlore structure type is that the $O(2)La_2$ anti-cristobalite network is but one of two interpenetrating (but not independent) networks comprising the pyrochlore structure type. The question of how coupled tetrahedral edge rotation of the OLa_2 anti-cristobalite network might affect the second Zr_2O_6 "octahedral" network is far from immediately apparent, although there is certainly no good crystal chemical reason requiring rigid ZrO_6 "octahedra" (16).

In the case of so-called stuffed cristobalite structures, it is known that description in terms of ⟨110⟩ tetrahedral edge rotation of framework tetrahedra remains a good approximation as long as the bonding interactions between the framework ions of the tetrahedra are significantly stronger than any bonding interactions of framework ions with interstitial ions (17). The strongest interaction between the two component networks in the case of the pyrochlore structure type is between the La^{3+} ions of the $O(2)La_2$ network and

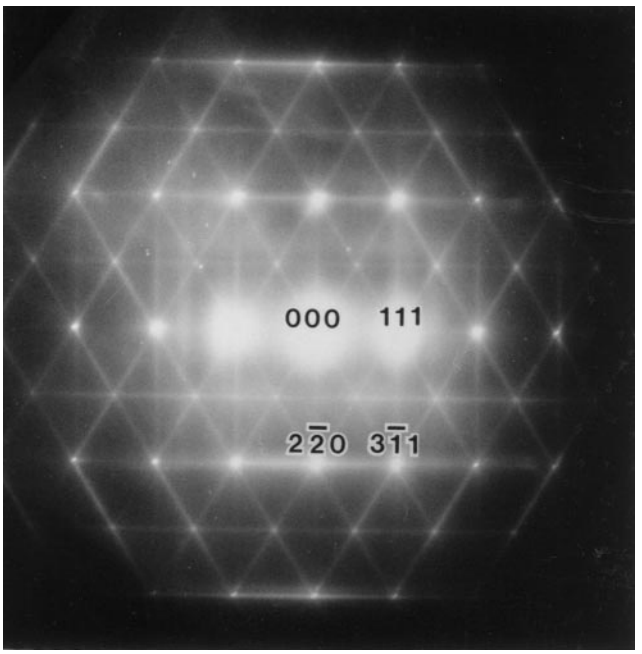

FIG. 4. ⟨112⟩ zone axis EDP of β-cristobalite (compare with Fig. 3b).

the $O(1)^{2-}$ ions of the Zr_2O_6 network. The strength of this interaction is indeed significantly weaker than the interaction between O(1) and La within the tetrahedra, suggesting that ⟨110⟩ tetrahedral edge rotation of the $O(2)La_2$ network should likewise remain a good approximation.

DISCUSSION

In attempting to rationalize the above-reported behavior, it is important to recognize that the pyrochlore structure type is overdetermined in that it is not possible to simultaneously satisfy the bonding requirements of all four independent ions per unit cell given that there are only two structural degrees of freedom, namely the x fractional coordinate of O(1) and the cubic unit cell parameter (12). Figure 6a, for example, shows calculated bond valence sums (V_i's (18)) for the four independent ions of the $La_2Zr_2O_7$ pyrochlore structure type as a function of the x fractional coordinate of O(1).

Note that the V_i of O(2) is independent of x while that of O(1) is only weakly dependent upon x. By contrast the V_i's of the metal ions are strongly dependent upon x. The observed value for x of 0.330 (19, 20) can be seen to be a compromise between the ideal value as far as the La^{3+} ions are concerned of 0.333 and the ideal value as far as the Zr^{4+} ions are concerned of 0.327. The compromise value of 0.330 leads to the La^{3+}, Zr^{4+}, and $O(1)^{2-}$ ions all being somewhat underbonded ($V_i(La) = 2.92$, $V_i(Zr) = 3.90$, $V_i(O(1)) = 1.85$) and the $O(2)^{2-}$ ion being rather more significantly overbonded ($V_i(O(2)) = 2.55$ instead of 2.0); i.e., the La^{3+}–O^{2-} bonds are too short (2.34 Å instead of the ideal 2.43 Å). Note further that the La–La separation distances within the $O(2)La_4$ tetrahedra are likewise quite short (3.82 Å as opposed to 3.75 Å in elemental close packed lanthanum and 3.86 Å in $La(OH)_3$). The V_i of O(2) can only

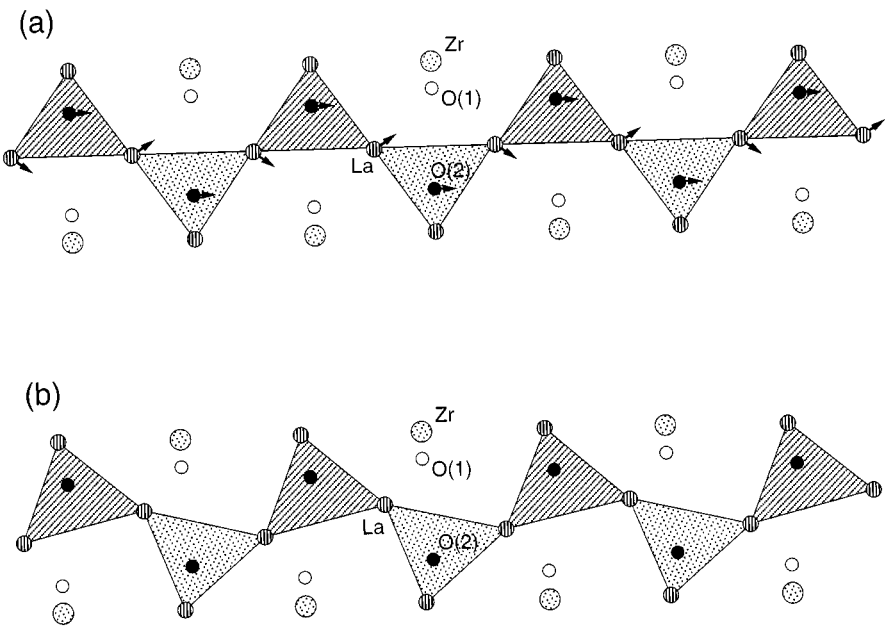

FIG. 5. Coupled rotation of framework tetrahedra about their ⟨110⟩ tetrahedral edges (as shown) is the natural "normal mode" for β-cristobalite related structures. (a) Atomic displacements associated with tetrahedral edge rotation about one particular ⟨110⟩ axis (out of the page). (b) Resultant structure of the $O(2)La_4$ column after the rotation. The "interstitial" Zr and O(1) ions are shown in their ideal pyrochlore average positions.

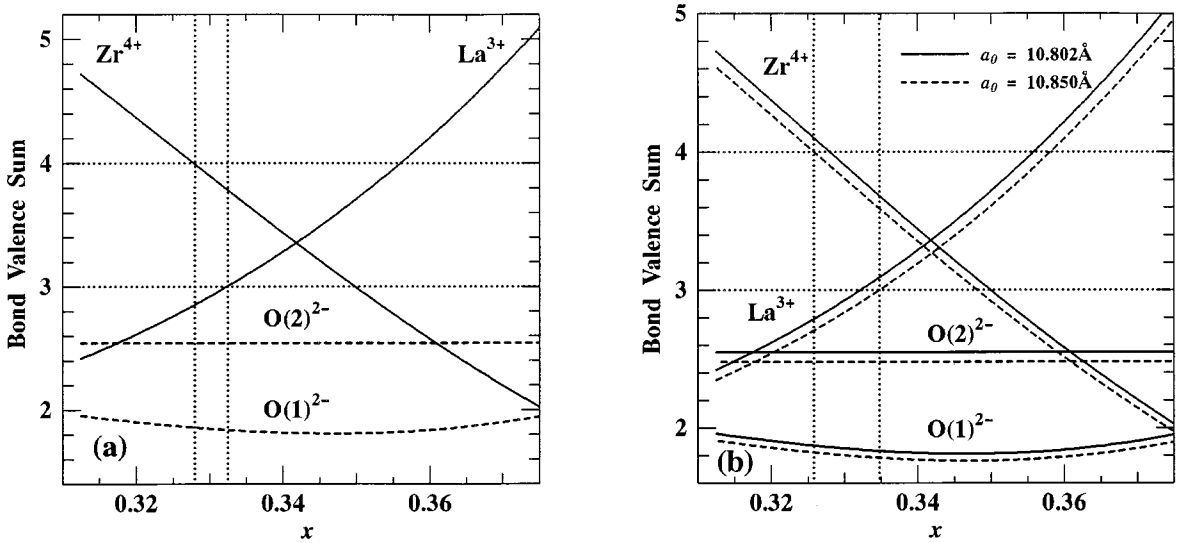

FIG. 6. (a) Bond valence sums, V_i's, for the four independent ions of the $La_2Zr_2O_7$ pyrochlore structure type as a function of the x fractional coordinate of O(1). (b) Increasing the cubic unit cell parameter reduces the overbonding of the $O(2)^{2-}$ ion. It also, however, simultaneously reduces the underbonding of the La^{3+} and Zr^{4+} ions.

be reduced by increasing the size of the $O(2)La_4$ tetrahedra. One way of achieving this is via a simple expansion of the cubic unit cell parameter. This, however, simultaneously increases the underbonding of the La^{3+}, Zr^{4+}, and $O(1)^{2-}$ ions by reducing their V_i's still further (see Fig. 6b). The overall crystal chemistry cannot be improved by such a unit cell expansion.

An alternative way of increasing the size of the $O(2)La_4$ tetrahedra is via $\langle 110 \rangle$ tetrahedral edge rotation of the type shown in Fig. 5. Such a rotation, for a fixed unit cell dimension, automatically expands the size of the $O(2)La_4$ tetrahedra and hence reduces the overbonding of the O(2) ions. In addition, such a rotation leads to La^{3+} ions moving more or less directly away from one $O(1)^{2-}$ ion and directly toward another in a neighboring $O(1)La_2Zr_2$ tetrahedra (see Fig. 5). A 0.2 Å shift of the La ions, for example, leads to an $\sim$0.1 increase in the V_i's of both La and O(1) if the O(1) ion does not move in response to the La ion shifts, i.e., the rotation simultaneously also improves the underbonding of the La and O(1) ions. Note that a larger amplitude shift of the La ions could be accommodated for the same increase in AV of the La and O(1) ions if the O(1) ions were to simultaneously move in the same direction as the O(2) ion (see Fig. 5a). If the O(1) ion were also to relax slightly toward the two neighboring Zr ions or vice versa then the underbonding of the Zr ions could also be reduced. It is difficult to discuss the relaxation of the Zr and O(1) ions in more detail, as this will depend upon the pattern of tetrahedral edge rotation from one $\langle 110 \rangle$ column of $O(2)La_4$ tetrahedra to the next. Nonetheless it would seem that tetrahedral edge rotation of the sort shown in Fig. 5, in conjunction with some small amplitude relaxation of neighboring Zr and O(1) ions, is indeed capable of improving the overall crystal chemistry of the pyrochlore structure type.

From a nonbonded metal–metal point of view such tetrahedral edge rotation would obviously give rise to a range of La–Zr separation distances, some shorter and some larger than the 3.82 Å separation distance of the average structure. Given that the minimum Zr^{4+}–Zr^{4+} separation distance in monoclinic ZrO_2 is $\sim$3.33 Å while the minimum La^{3+}–La^{3+} separation distance in $La(OH)_3$ is 3.86 Å, it is clear that there is considerable scope for tetrahedral edge rotation of the type shown in Fig. 5 before nonbonded metal–metal interactions could be expected to come into play. Such considerations suggest that the amplitude of the tetrahedral edge rotation is likely to be controlled by the size difference between the constituent metal ions of the particular pyrochlore.

Note that this size difference between the Ln^{3+} and Zr^{4+} ions is also likely to play an important role in determining the experimental extent of the pyrochlore solid solution. An La^{3+} ion in a Zr^{4+} site, for example, would have a V_i of 7.37, whereas a Zr^{4+} ion in an La^{3+} site would have a V_i of 1.55 without local rearrangement. Given the magnitude of this overbonding of a La^{3+} ion in a Zr^{4+} site and underbonding of a Zr^{4+} ion in an La^{3+} site, it is not surprising that the extent of the pyrochlore solid solution in the case of $Ln =$ La is extremely narrow. As the size of the lanthanide reduces, however, the extent of this over- and underbonding also reduces so that it is crystal chemically reasonable to expect the extent of the pyrochlore solid solution to increase in going from $Ln =$ La to Gd.

Symmetry lowering as a result of $\langle 110 \rangle$ tetrahedral edge rotations of the type shown in Fig. 5 could be expected only if a particular pattern of rotations were to freeze in. The experimental existence of diffuse sheets of intensity perpendicular to the $\langle 110 \rangle$ directions in $La_2Zr_2O_7$ shows, as for β-cristobalite itself (16, 17), that no one such rotation pattern predominates, i.e., all rotation patterns must occur equally frequently when time and space averaged. The overall average $Fd3m$ cubic symmetry of $La_2Zr_2O_7$ is therefore apparently not due to the essential rigidity of the ideal pyrochlore structure type but rather, as for β-cristobalite itself (14–17), a result of its inability to choose between a myriad of distinct possible derivative structures.

ACKNOWLEDGMENT

The award of an Australian Research Council (ARC) post-doctoral fellowship to Y.T. is gratefully acknowledged.

REFERENCES

1. A. W. Sleight, *Inorg. Chem.* **7,** 1704 (1968).
2. M. A. Subramanian, G. Aravamudan, and G. V. Subba Rao, *Prog. Solid State Chem.* **15,** 55 (1983).
3. M. A. Subramanian and A. W. Sleight, *in* "Handbook on the Physics and Chemistry of the Rare Earths," vol. 16, pp. 225. 1993.
4. M. Perez y Jorba, *Ann. Chim.* (*Paris*) **7,** 509 (1962).
5. M. Faucher and P. Caro, *J. Solid State Chem.* **12,** 1 (1975).
6. D. Michel, M. Perez y Jorba, and R. Collongues, *J. Raman Spectrosc.* **5,** 163 (1976).
7. R. Collongues, F. Queyroux, M. Perez y Jorba, and J.-C. Gilles, *Bull. Soc. Chim. Fr.* **4,** 1141 (1965).
8. A. Rouanet, *Rev. Int. Hautes Temp. Refract.* **8,** 161 (1971).
9. R. L. Withers, J. G. Thompson, P. J. Barlow, and J. C. Barry, *Aust. J. Chem.* **45,** 1375 (1992).
10. R. L. Withers, J. G. Thompson, and P. J. Barlow, *J. Solid State Chem.* **94,** 89 (1991).
11. M. P. van Dijk, F. C. MIjlhoff, and A. J. Burggraaf, *J. Solid State Chem.* **62,** 377 (1986).
12. B. G. Hyde, J. G. Thompson, and R. L. Withers, *in* "Structure and Properties of Ceramics" (M. Swain Ed.), p. 1, Materials Science and Technology (R. Cahn, P. Haasen, and E. Kramer, Eds.), vol. 11. VCH, Weinheim, 1993.
13. T. R. Welberry, *Rep. Prog. Phys.* **48,** 1543 (1985).
14. G. L. Hua, T. R. Welberry, R. L. Withers, and J. G. Thompson, *J. Appl. Crystallogr.* **21,** 458 (1988).
15. R. L. Withers, J. G. Thompson, and T. R. Welberry, *Phys. Chem. Miner.* **16,** 517 (1989).
16. R. L. Withers, S. Schmid, and J. G. Thompson, *Prog. Solid State Chem.* **26,** 1 (1998).
17. J. G. Thompson, R. L. Withers, S. R. Palethorpe, and A. Melnitchenko, *J. Solid State Chem.*, in press.
18. N. E. Brese and M. O'Keeffe, *Acta Crystallogr. B* **47,** 192 (1991).
19. H. J. Deiseroth and H. Müller-Buschbaum, *Z. Anorg. Allg. Chem.* **375,** 152 (1970).
20. Y. Tabira and R. L. Withers, *Phil. Mag. A*, in press.